

# Nanoscale

Accepted Manuscript



This is an *Accepted Manuscript*, which has been through the Royal Society of Chemistry peer review process and has been accepted for publication.

*Accepted Manuscripts* are published online shortly after acceptance, before technical editing, formatting and proof reading. Using this free service, authors can make their results available to the community, in citable form, before we publish the edited article. We will replace this *Accepted Manuscript* with the edited and formatted *Advance Article* as soon as it is available.

You can find more information about *Accepted Manuscripts* in the [Information for Authors](#).

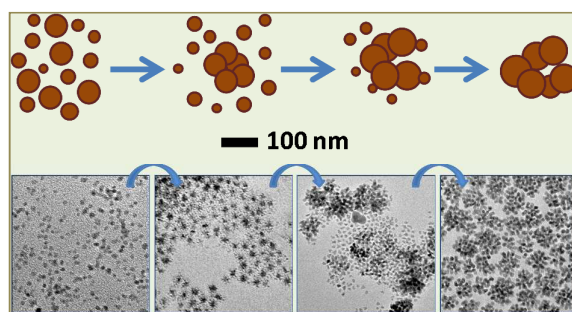
Please note that technical editing may introduce minor changes to the text and/or graphics, which may alter content. The journal's standard [Terms & Conditions](#) and the [Ethical guidelines](#) still apply. In no event shall the Royal Society of Chemistry be held responsible for any errors or omissions in this *Accepted Manuscript* or any consequences arising from the use of any information it contains.

Graphic abstract

## A universal approach to the synthesis of nanodendrites of noble metals

Yan Feng,<sup>ab</sup> Xiaohong Ma,<sup>a</sup> Lin Han,<sup>ac</sup> Zhijian Peng<sup>c</sup> and Jun Yang<sup>a\*</sup>

A universal approach was demonstrated for the synthesis of noble metal nanoparticles with dendritic structures.



Cite this: DOI: 10.1039/c0xx00000x

www.rsc.org/xxxxxx

ARTICLE TYPE

# A universal approach to the synthesis of nanodendrites of noble metals<sup>†</sup>

Yan Feng,<sup>ab</sup> Xiaohong Ma,<sup>a</sup> Lin Han,<sup>ac</sup> Zhijian Peng<sup>c</sup> and Jun Yang<sup>a\*</sup>

Received (in XXX, XXX) Xth XXXXXXXXX 20XX, Accepted Xth XXXXXXXXX 20XX

DOI: 10.1039/b000000x

5 Nanomaterials usually exhibit structure-dependent catalytic activity, selectivity, and stability. Herein, we report a universal approach for the synthesis of noble metal nanoparticles with dendritic structures, which is based on the reduction of metal acetylacetonate precursors in oleylamine at a temperature of 160°C. In this strategy, the metal acetylacetonate precursors are reduced into metal atoms by oleylamine and grow into metal nanoparticles, while oleylamine is simultaneously converted into oleylamide to protect the  
10 nanoparticles. The competition between particle aggregation and the oleylamide passivation is essential to form a large number of particle aggregates, which eventually grow into nanodendrites *via* Ostwald ripening process. In particular, in comparison with the commercial PtRu/C catalysts, the alloy PtRuOs nanodendrites displayed superior catalytic activity toward methanol oxidation.

## 1 Introduction

15 Noble metal nanomaterials with dendritic structures have garnered sustained research interest for their high catalytic performance, which is usually stemmed from the porous structure, large specific surface area, many hot catalytic spots, and high-index exposed facets etc.<sup>1–8</sup> For instance, bimetallic Pt-on-Pd  
20 nanodendrites with enhanced catalytic activity for oxygen reduction reaction have been reported.<sup>9–12</sup> The synthesis of such electrocatalysts starts with the preparation of truncated Pd cores through wet chemistry. A dense array of Pt branches are formed subsequently onto the Pd cores from the metal precursors via a  
25 facet-selective growth. Most recently, Mourdikoudis and co-workers reported a dimethylformamide-mediated strategy for the synthesis of Pt nanodendrites, which could be well dispersed in aqueous phase in the presence of polyethyleneimine, and displayed excellent performance in catalyzing ethanol oxidation.<sup>13</sup>

30 Up to date, a number of strategies upon thermal decomposition of metal precursors in high-boiling solvents,<sup>14</sup> self-organization,<sup>15</sup> pH controlling,<sup>16</sup> electrochemical synthesis,<sup>17</sup> and seed-mediated growth<sup>18–20</sup> have been developed for the synthesis of monometallic or bimetallic nanodendrites. In an early study,  
35 Yang and co-workers described the synthesis of porous Pt nanodendrites in a mixture consisting of diphenyl, 1,2-hexadecanediol, hexadecylamine, and 1-adamantanecarboxylic acid, which were used as solvent, reducing reagent, surfactant, and co-ordinating agent, respectively.<sup>15</sup> Most recently, we  
40 reported a general approach, which is based on preferential nucleation and growth of noble metals on the active twins of Au seed particles, for the fabrication of bimetallic nanoparticles with dendritic structures.<sup>21</sup> In this strategy, the Au nanoparticles with multiple twins were formed firstly, and served as seeds for the  
45 subsequent nucleation and growth of other noble metals, resulting in the formation of bimetallic Au-noble metal nanodendrites,

which displayed superior catalytic activity toward methanol oxidation reaction (MOR) for the presence of unique dendritic structures, as compared with that of commercial Pt/C catalysts.

50 Considering the great potential of these dendritic nanostructures in many catalytic applications, the production of noble metal nanodendrites (NMNDs) consisting of a wide spectrum of noble metals would be undoubtedly important and pose significant challenges. In the present work, we present a  
55 universal, facile, and high-yield approach to the synthesis of noble metal nanodendrites including Pt, Pd, Ru, Rh, Ir, PtPd, PtRh, PtIr, PtPdRu, PtPdRh, PtRuOs, and PtRhOs, labeled as NMNDs, which is based on the oleylamine reduction of suitable metal precursors at a certain temperature. This synthetic pathway  
60 does not rely on any additional templates, ion replacements, or substrates. The novelty of this approach lies in its remarkable simplicity, universality, and a competing mechanism we proposed to interpret the formation of noble metal nanodendrites. In particular, the catalytic activities of the Pt-containing NMNDs  
65 toward methanol oxidation reaction (MOR) are examined and compared. This study might provide a promising method with remarkable simplicity and universality for creating heterogeneously structured nanomaterials for given technological applications.

## 2 Experimental

### 2.1 General materials

Platinum(II) acetylacetonate (Pt(acac)<sub>2</sub>, 97%), potassium tetrachloroplatinate(II) (K<sub>2</sub>PtCl<sub>4</sub>, 98%), palladium(II) acetylacetonate (Pd(acac)<sub>2</sub>, 99%), palladium(II) chloride (PdCl<sub>2</sub>,  
75 99%), ruthenium(III) acetylacetonate (Ru(acac)<sub>3</sub>, 97%), rhodium(III) acetylacetonate (Rh(acac)<sub>3</sub>, 97%), iridium(III) acetylacetonate (Ir(acac)<sub>3</sub>, 97%), and osmium(III) acetylacetonate (Os(acac)<sub>3</sub>, 97%) from Sigma-Aldrich, aqueous HClO<sub>4</sub> solution (70%, ACS reagent) and Nafion 117 solution (5% in a mixture of

lower aliphatic alcohols and water) from Aladdin Reagents, oleylamine (95.4%, primary amine) from J&K Scientific, methanol (99%) and toluene (99.5%) from Beijing Chemical Works, and Vulcan XC-72 carbon powders (XC-72C, BET surface area = 250 m<sup>2</sup>/g and average particle size = 40~50 nm) from Cabot Corporation, were used as received. All glassware and Teflon-coated magnetic stir bars were cleaned with *aqua regia*, followed by copious washing with de-ionized water before drying in an oven.

## 2.2 Synthesis of noble metal nanodendrites (NMNDs)

The synthesis of NMNDs was conducted in oleylamine using metal acetylacetonate as the precursor. In typical synthesis of monometallic nanodendrites, 0.5 mmol of Pt(acac)<sub>2</sub>, Pd(acac)<sub>2</sub>, Ru(acac)<sub>3</sub>, Rh(acac)<sub>3</sub>, Ir(acac)<sub>3</sub>, or Os(acac)<sub>3</sub> was added to 20 mL of oleylamine in a three-necked flask equipped with a condenser and a stir bar. The solution was brought to and kept at 160°C for 2 h under flowing N<sub>2</sub> for the reduction of metal precursor by oleylamine.

For the synthesis of Pt-containing alloy NMNDs, 0.25 mmol Pt(acac)<sub>2</sub>/0.25 mmol Pd(acac)<sub>2</sub>, or 0.25 mmol Pt(acac)<sub>2</sub>/0.25 mmol Rh(acac)<sub>3</sub>, 0.25 mmol Pt(acac)<sub>2</sub>/0.25 mmol Ir(acac)<sub>3</sub>, 0.25 mmol Pt(acac)<sub>2</sub>/0.25 mmol Os(acac)<sub>3</sub>, 0.25 mmol Pt(acac)<sub>2</sub>/0.125 mmol Pd(acac)<sub>2</sub>/0.125 mmol Ru(acac)<sub>3</sub>, 0.25 mmol Pt(acac)<sub>2</sub>/0.125 mmol Pd(acac)<sub>2</sub>/0.125 mmol Rh(acac)<sub>3</sub>, 0.25 mmol Pt(acac)<sub>2</sub>/0.125 mmol Ru(acac)<sub>3</sub>/0.125 mmol Os(acac)<sub>3</sub>, 0.25 mmol Pt(acac)<sub>2</sub>/0.125 mmol Rh(acac)<sub>3</sub>/0.125 mmol Os(acac)<sub>3</sub> was added to 20 mL of oleylamine in a three-necked flask equipped with a condenser and a stir bar, followed by heating and keeping at 160°C for 2 h under flowing N<sub>2</sub> for the reduction of the metal precursors.

After reaction, both the monometallic and alloy nanodendrites were purified by precipitation with methanol, centrifugation, washing with methanol, and re-dispersed in 20 mL of toluene.

## 2.3 Particle characterizations

Transmission electron microscopy (TEM) and high resolution TEM (HRTEM) were performed on the JEOL JEM-2100 electron microscope operating at 200 kV with a supplied software for automated electron tomography. For the TEM measurements, a drop of the nanoparticle solution was dispensed onto a 3-mm carbon-coated copper grid. Excessive solution was removed by an absorbent paper, and the sample was dried under vacuum at room temperature. The average particle size and particle size distribution were obtained from a few randomly chosen areas in the TEM image containing ~200 nanoparticles each. An energy dispersive X-ray spectroscopy (EDX) analyzer attached to the TEM was used to analyze the chemical compositions of the synthesized NMNDs. Powder X-ray diffraction (XRD) patterns were recorded on a Rigaku D/Max-3B diffractometer, using Cu K<sub>α</sub> radiation (λ=1.54056 Å). Samples for XRD analyses were concentrated from the toluene solution of NMNDs to 0.5 mL using flowing N<sub>2</sub>. 10 mL of methanol was then added to precipitate the NMNDs, which were recovered by centrifugation, washed with methanol several times, and then dried at room temperature in vacuum.

## 2.4 Electrochemical measurements

Electrochemical measurements were carried out in a standard three-electrode cell connected to a Bio-logic VMP3 (with EC-lab software version 9.56) potentiostat. A leak-free Ag/AgCl (saturated with KCl) electrode was used as the reference electrode. The counter electrode was a platinum mesh (1×1 cm<sup>2</sup>) attached to a platinum wire.

For the loading of the Pt-containing NMNDs on Vulcan XC-72 carbon support, a calculated amount of carbon powder was added to the toluene solution of NMNDs. After stirring the mixture for 24 h, the NMNDs/C (20 wt% Pt on carbon support) was collected by centrifugation, washed thrice with methanol, and then dried at room temperature in vacuum.

The working electrode was a thin layer of Nafion-impregnated catalyst cast on a vitreous carbon disk. This electrode was prepared by ultrasonically dispersing 10 mg of the NMNDs/C in 10 mL of aqueous solution containing 4 mL of ethanol and 0.1 mL of Nafion. A calculated volume of the ink was dispensed onto the 5 mm glassy carbon disk electrode to produce a nominal catalyst loading of 20 μg cm<sup>-2</sup> (Pt basis). The carbon electrode was then dried in a stream of warm air at 70°C for 1 h.

The room temperature cyclic voltammograms of Pt-containing NMNDs in argon-purged HClO<sub>4</sub> (0.1 M) were recorded between -0.2 V and 0.8 V at 50 mV s<sup>-1</sup> and used for the determination of electrochemically active surface area (ECSA) of Pt. The catalyst performance in room-temperature methanol oxidation reaction (MOR) was also measured by cyclic voltammetry. For these measurements the potential window of 0 V to 1 V was scanned at 20 mV s<sup>-1</sup> until a stable response was obtained. The electrolyte was methanol (1 M) in perchloric acid (0.1 M), and the current density was normalized by the ECSA and total mass of the dendritic catalysts to obtain the specific activities.

## 3 Results and discussion

### 3.1 Monometallic NMNDs

Monometallic NMNDs including Pt, Pd, Ru, Rh, Ir, and Os could be produced by simply heating their acetylacetonate precursors in oleylamine with purity of 95.4%. No extra reducing agent and stabilizers are needed to achieve these syntheses. After reaction, the dendritic products were purified by precipitation with methanol, centrifugation, washing with methanol, and re-dispersed in toluene. As shown in Fig. S1 of Electronic Supplementary Information (ESI), the XRD patterns demonstrated the successful syntheses of hexagonal Ru and Os nanoparticles, and face-centred cubic (fcc) Pt, Pd, Rh, and Ir nanoparticles.<sup>22</sup> The dendritic feature of the monometallic nanoparticles were demonstrated by the TEM images in Fig. 1, which also showed that the NMNDs were uniform in size and had an overall average size of 25.6 nm for Pt (Fig. 1a), 30.5 nm for Pd (Fig. 1d), 16.7 nm for Ru (Fig. 1g), 24.4 nm for Rh (Fig. 1j), 22.2 nm for Ir (Fig. 1m), and 17.8 nm for Os (Fig. 1p), respectively. The synthetic parameters, average size, and size distributions of the monometallic NMNDs were summarized in ESI Table S1.

The dendritic nature of the NMNDs was further revealed by the high-resolution TEM (HRTEM) images of six individual particles (Fig. 1b, e, h, k, n, and q for Pt, Pd, Ru, Rh, Ir, and Os, respectively), which demonstrated that each dendritic particle was actually composed of a number of small particles. The presence

of the corresponding noble metals in the NMNDs was confirmed by the results of EDX analyses (Fig. 1c, f, i, l, o, and r) of these six monometallic nanosystems.

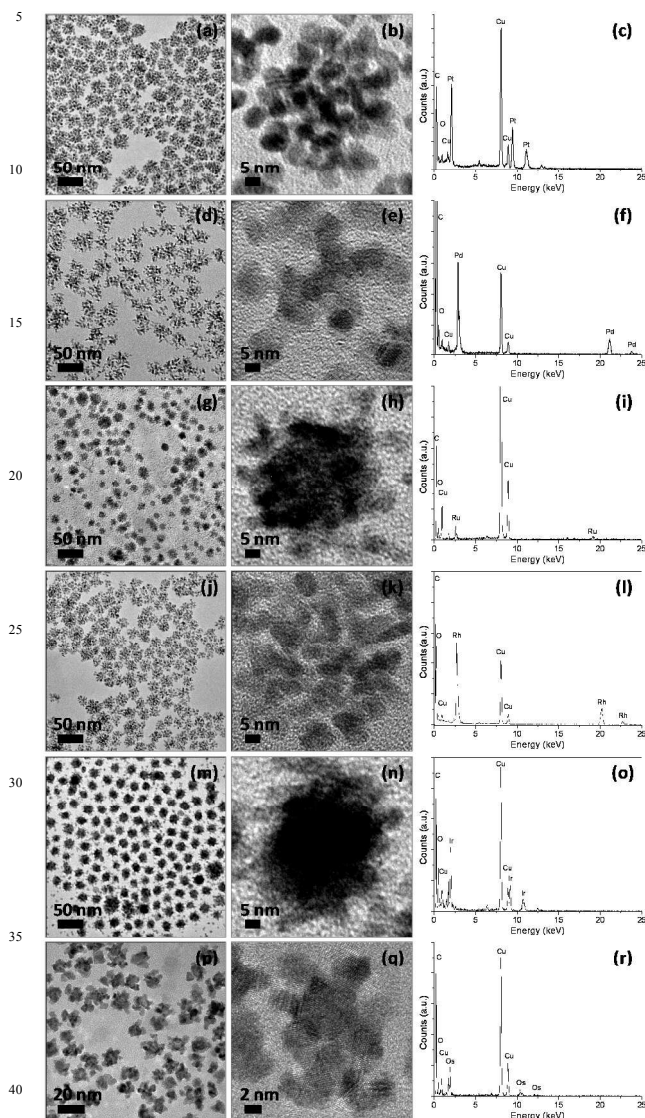


**Fig. 1** TEM image (a,d,g,j,m,p), HRTEM image (b,e,h,k,n,q), and EDX analyses (c,f,i,l,o,r) of the Pt (a,b,c), Pd (d,e,f), Ru (g,h,i), Rh (j,k,l), Ir (m,n,o), and Os nanodendrites (p,q,r) synthesized in oleylamine at 45 temperature of 160°C.

### 3.2 Mechanism for the formation of NMNDs

We will use monometallic Pt nanosystem as a typical example to elucidate the mechanism for the formation of NMNDs. TEM of the aliquots taken out from the reaction mixture at different time was monitored to follow the growth process of the Pt particles with dendritic morphologies. The results were shown in Fig. 2. After the reduction of Pt(acac)<sub>2</sub> in oleylamine at 160°C for 5 min, only spherical Pt nanoparticles with average size of 2.2 nm were observed in TEM image (Fig. 2a). After reaction for 20 min, in addition to the isolated small Pt particles, a large number of particle aggregates were appeared, as displayed by the TEM

image in Fig. 2b. After 60 min, the growth of Pt particle aggregates was detected by TEM (Fig. 2c). The final product was Pt nanodendrites with an average size of 25.6 nm (Fig. 2d) and a structure distinctively different from the spherical Pt nanoparticles formed at the early stage of the reaction.

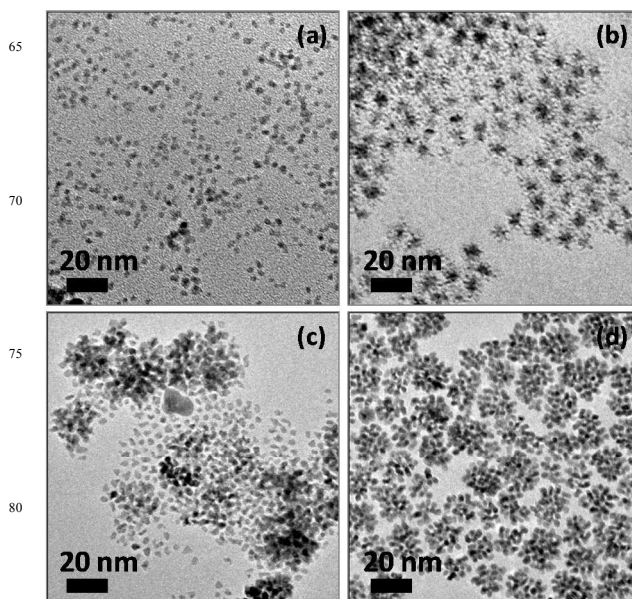


**Fig. 2** Representative TEM images of the Pt nanodendrites made after the 85 reduction of Pt(acac)<sub>2</sub> in oleylamine at 160°C for 5 min (a), 20 min (b), 60 min (c), and 120 min (d).

Amine is a common reducing agent for the synthesis of metal nanoparticles.<sup>23–27</sup> According to Huo and co-workers,<sup>28</sup> amine ligands are oxidized to amides in metal precursor reduction and form a protecting layer of hydrogen bond network on the metal nanoparticles. Therefore, the mechanism for the fabrication of NMNDs in oleylamine could be summarized by the scheme in Fig. 3. At initial stage, the metal acetylacetonate precursors were reduced into metal atoms by oleylamine and grew into metal nanoparticles, while oleylamides were simultaneously generated from oleylamine as the capping agent to stabilize the nanoparticles. Then the particle aggregation would compete with the oleylamide passivation, resulting in the formation of a large number of particle aggregates in the solution (step (a) in Fig. 3). Finally, the particle aggregates continuously grew with the expense of small nanoparticles in solution *via* a ripening process, e.g. Ostwald ripening,<sup>29</sup> to form larger and more stable nanodendrites (step (b) and (c) in Fig. 3).

The competition between particle aggregation and oleylamide passivation at initial stage of the synthesis was essential for the formation of NMNDs, which might be affected by the type of metal precursor and reaction temperature since the ligand in different metal precursors and the temperature would have significant influence on the reduction kinetics of the noble metal ions. For examples, concerning the Pt(acac)<sub>2</sub> and K<sub>2</sub>PtCl<sub>4</sub> as metal precursors, the acetylacetonate ion in Pt(acac)<sub>2</sub> and Cl<sup>-</sup> ions in K<sub>2</sub>PtCl<sub>4</sub> may have different effect on the reduction of Pt(II) ions, and therefore affect the competition between the aggregation and oleylamide passivation of Pt particles, resulting

in Pt with different morphologies. As two typical examples, for the Pt and Pd nanoparticles synthesized in oleylamine at 160°C using  $K_2PtCl_4$  and  $PdCl_2$  as metal precursors, respectively, there were no Pt and Pd nanodendrites, and Pt multipods and Pd network aggregates were formed, as shown in ESI Fig. S2. On the other hand, when the syntheses were carried out at temperature of 180°C with metal acetylacetonates as precursors, as indicated by the TEM and HRTEM images in ESI Fig. S3, Pt nanoparticles with irregular morphologies and large Pd aggregates were the majority products instead of Pt and Pd nanodendrites. Analogously, since the particle aggregation and oleylamide generation are varied at different temperature. The temperature could influence the morphology of the final metal products through affecting the competition between the aggregation and oleylamide passivation of noble metal particles.

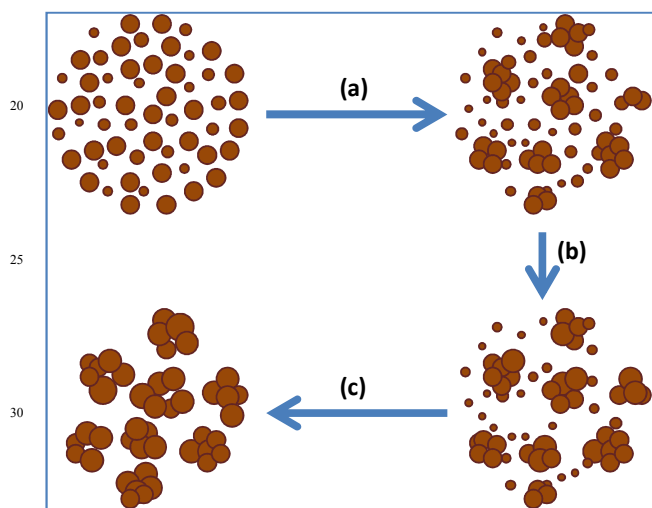


**Fig. 3** Schematic illustration to demonstrate the mechanism for the formation of NMNDs *via* the reduction of metal precursors in oleylamine at elevated temperature: (a) Competition between particle aggregation and oleylamide passivation results in the formation of particle aggregates; (b,c) particle aggregates grow into nanodendrites *via* Ostwald ripening.

### 3.3 Alloy nanodendrites of noble metals

The strategy in Fig. 3 was universal for the generation of alloy nanodendrites of noble metals. The syntheses involved co-reduction of two or more acetylacetonate precursor metals in oleylamine at temperature of 160°C in order to form alloy NMNDs. We will use PtRh nanosystem as a typical example to illustrate the characterization of these alloy NMNDs. Fig. 4a and 4b showed the TEM and HRTEM images of the alloy PtRh nanodendrites as-prepared by co-reduction of  $Pt(acac)_2$  and  $Rh(acac)_3$  in oleylamine at 160°C, which were found to consist of well dispersed nanoparticles with dendritic structures, manifesting the high-yield output of the NMNDs (approximate 100%). The alloy PtRh nanodendrites were uniform in size and had an overall average size of 24.8 nm. The distribution of Pt and Rh in the NMNDs was investigated by EDX analysis under high-angle annular dark-field scanning TEM (HAADF-STEM) mode. Nanoscale element mapping of two particles (Fig. 4c) revealed that Pt and Rh were distributed uniformly throughout the entire

particle (Fig. 4d–f). The EDX line scanning analysis of two arbitrary particles (Fig. 4g) also showed that the Pt and Rh signals were across the entire particle (Fig. 4h). The EDX analysis produced a Pt/Rh molar ratio of 54/46, which is in good agreement with the metal ratio in the starting precursors. Another example to confirm the formation of alloy nanodendrites by co-reduction of two acetylacetonate precursors in oleylamine was presented in ESI Fig. S4, which displayed the characterizations of alloy PtIr nanosystem.

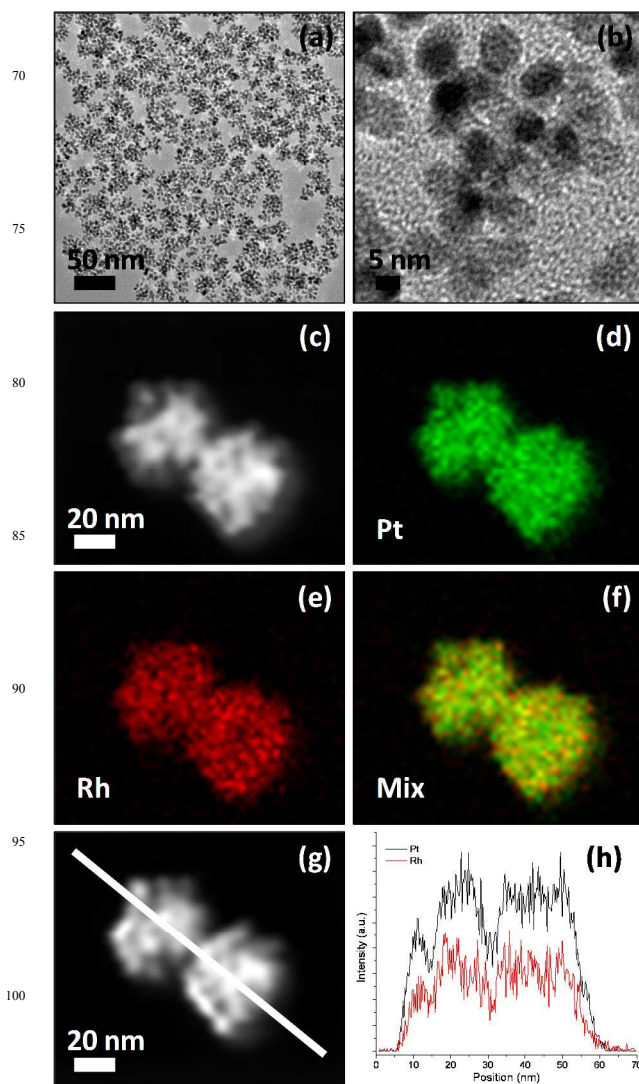


**Fig. 4** TEM image (a), HRTEM image (b), elemental mapping (c–f), and line scanning analysis (g,h) of PtRh nanodendrites synthesized in oleylamine at 160°C using  $Pt(acac)_2$  and  $Rh(acac)_3$  as metal precursors.

The TEM (ESI Fig. S5a, c, e, g, i, and k) and HRTEM images (ESI Fig. S5b, d, f, h, j, and l) of other alloy NMNDs including PtPd (ESI Fig. S5a and b), PtOs (ESI Fig. S5c and d), PtPdRu (ESI Fig. S5e and f), PtPdRh (ESI Fig. S5g and h), PtRuOs (ESI Fig. S5i and j), and PtRhOs (ESI Fig. S5k and l) showed that only nanoparticles with dendritic structures were obtained in the final products. The synthetic parameters, average size, and size distributions of these alloy nanodendrites were also listed in ESI

Table S1. The presence of the corresponding noble metals in the alloy NMNDs was confirmed by the results of EDX analyses (ESI Fig. S6a–f) of these six alloy nanosystems. The molar ratios of the corresponding noble metals in these alloy NMNDs

obtained by EDX analyses were listed in ESI Table S2, and as indicated, they are also in good agreement with the metal ratios in the starting precursors. In comparison with the dendritic nanostructures formed through either Stranski-

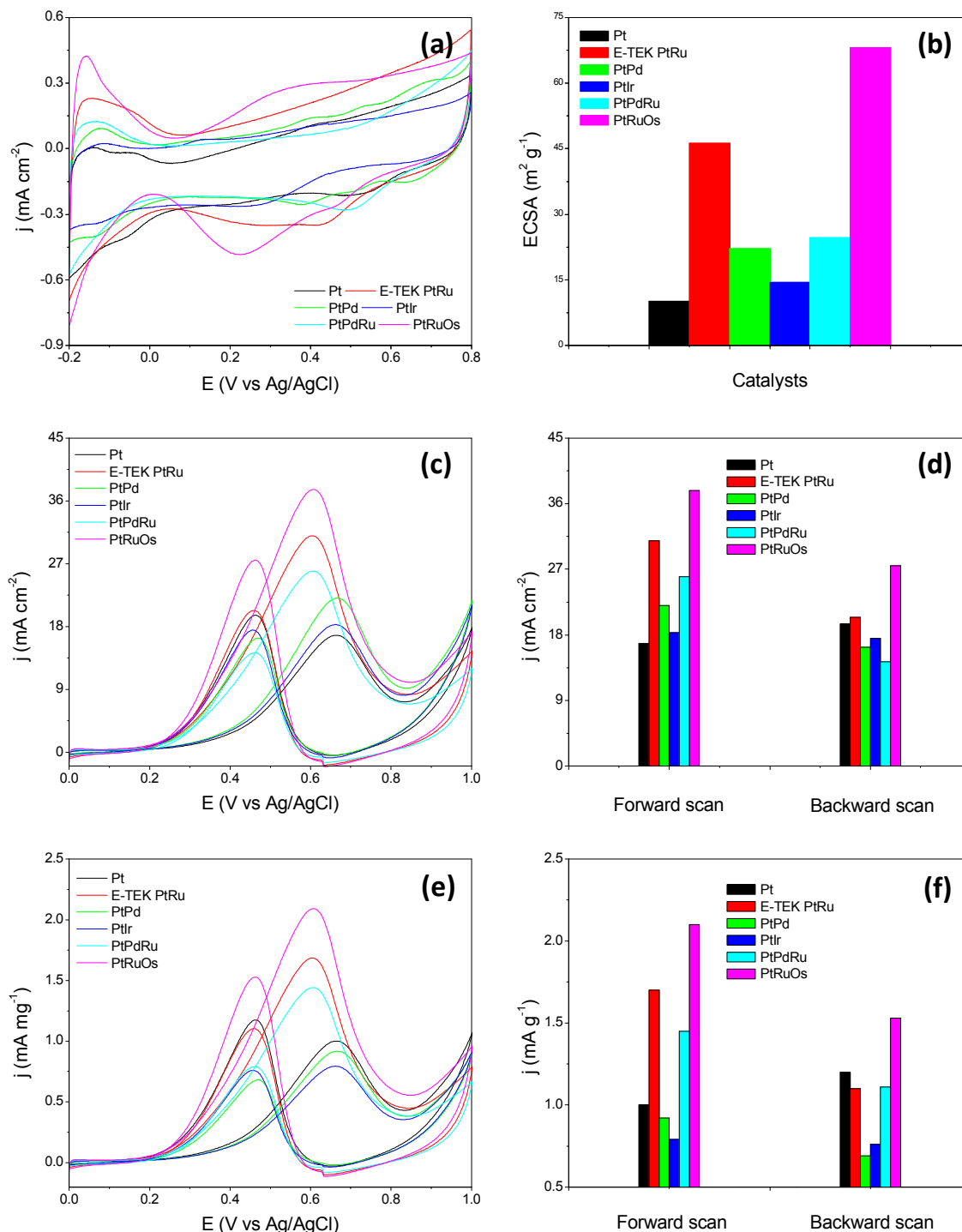


**Fig. 5** Cyclic voltammograms of Pt-containing NMNDs in argon-purged  $\text{HClO}_4$  (0.1 M) with sweeping rate of  $50 \text{ mV s}^{-1}$  (a); histogram to summarize the ECSA of Pt-containing NMNDs (b); ECSA-based cyclic voltammograms of Pt-containing NMNDs in argon-purged  $\text{HClO}_4$  (0.1 M) with methanol of 1 M and sweeping rate of  $20 \text{ mV s}^{-1}$  (c); histogram to summarize the ECSA-based current densities of Pt-containing NMNDs associated with methanol oxidation in the forward and reverse scans (d); mass-based cyclic voltammograms of Pt-containing NMNDs in argon-purged  $\text{HClO}_4$  (0.1 M) with methanol of 1 M and sweeping rate of  $20 \text{ mV s}^{-1}$  (e); and histogram to summarize the mass-based current densities of Pt-containing NMNDs associated with methanol oxidation in the forward and reverse scans (f).

Krastanov or Volmer-Weber mode,<sup>30</sup> the present synthesis in oleylamine shows remarkable simplicity and universality. In addition, the mechanistic understanding for the fabrication of NMNDs from the competition between particle aggregation and oleylamide passivation might be used to design and generate other heterogeneous nanostructures for wide application explorations.

### 3.4 Electrochemical property of the Pt-containing NMNDs

We characterized the electrocatalytic activities of a number of Pt-containing NMNDs toward the room temperature methanol oxidation reaction (MOR) and benchmarked with that of commercial PtRu/C catalysts (E-TEK, alloy PtRu nanoparticles (~3.5 nm) on Vulcan XC-72 carbon support, ESI Fig. S7). The electrochemically active surface areas (ECSAs) of the Pt-containing NMNDs were determined using cyclic voltammetry, as shown in Fig. 5a. The specific ECSAs, based on the unit weight of Pt and calculated by integrating the charge associated with the hydrogen adsorption/desorption potential region after double-layer correction, were 10.08 m<sup>2</sup> g<sub>Pt</sub><sup>-1</sup> for Pt, 46.24 m<sup>2</sup> g<sub>Pt</sub><sup>-1</sup> for E-TEM PtRu/C, 22.2 m<sup>2</sup> g<sub>Pt</sub><sup>-1</sup> for PtPd, 14.44 m<sup>2</sup> g<sub>Pt</sub><sup>-1</sup> for PtIr, 24.64 m<sup>2</sup> g<sub>Pt</sub><sup>-1</sup> for PtPdRu, and 68.05 m<sup>2</sup> g<sub>Pt</sub><sup>-1</sup> for PtRuOs NMNDs, respectively, as summarized in Fig. 5b. The differences in ECSAs among the Pt-containing NMNDs were most likely due to the presence of residual impurities adsorbed on the surface, different overall size of the NMNDs, and different particle sizes and porosities in the NMNDs.

The ECSA- and mass-based voltammograms of methanol oxidation shown in Fig. 5c and 5e, respectively, were obtained in the potential window of 0–1 V at a sweeping rate of 20 mV s<sup>-1</sup>. The current densities were summarized by the histograms in Fig. 5d and 5f, respectively. From the comparison of current densities, the Pt-containing alloy NMNDs showed higher catalytic activities than that of Pt nanodendrites. It was worthy to note that the PtRuOs nanodendrites particles always display the highest catalytic activity for MOR, definitely supporting that the introduction of Os to the traditional Pt-containing alloy nanomaterials is an effective way to prepare high efficient catalysts toward MOR in direct methanol fuel cell,<sup>31,32</sup> although the effect of the dendritic structure on the catalytic activity of the alloy nanomaterials cannot be ruled out. Os is supposed to modify the adsorptive properties of alloy PtRu towards oxygen-containing species at potentials slightly more negative than for Ru.<sup>33</sup> According to the bi-functional catalysis,<sup>34,35</sup> a timely supply of oxygen-containing species would be helpful to reduce the adsorption of CO-like species, which are the intermediate products during MOR and are the catalyst poisons, on the Pt particles, therefore PtRuOs nanoparticles are superior to pure Pt or other Pt-containing alloy electrocatalysts. The long-term performance of the Pt-containing NMNDs in methanol oxidation was illustrated in the chronoamperograms in ESI Fig. S8. The slower rate of decay for the PtRuOs nanodendrites also indicated their better catalytic stability to that of other Pt-containing alloy NMNDs.

The TEM and HRTEM images of a number of typical nanodendrites (Pt, PtPd, PtIr, and PtRuOs) before and after electrochemical measurements were shown by ESI Fig. S9. As exhibited, no apparent change in size and morphology could be

observed in comparison with those of the particles displayed in Fig. 1 and ESI Fig. S5, indicating the high structural stability during the electrochemical measurement.

## 4 Conclusions

In summary, we have developed a universal approach for the fabrication of noble metal nanoparticles with dendritic structures, which was based on the oleylamine reduction of metal acetylacetonate precursors at a temperature of 160°C. In this strategy, the metal acetylacetonate precursors were reduced into metal atoms by oleylamine and grew into metal nanoparticles, while oleylamine was simultaneously converted into oleylamide to protect the nanoparticles. The competition between particle aggregation and the oleylamide passivation resulted in the formation of a large number of particle aggregates, which were eventually grown into nanodendrites with the expense of small nanoparticles in solution *via* Ostwald ripening process. This synthetic pathway does not rely on any additional templates, ion replacements, or substrates. In particular, in comparison with the commercial PtRu/C catalysts, the alloy PtRuOs nanodendrites displayed superior catalytic activity toward methanol oxidation. The synthetic universality and mechanistic understanding make this work a significant advance in producing heterogeneously structured nanomaterials for given technological applications.

## Acknowledgement

Financial support from the 100 Talents Program of the Chinese Academy of Sciences, National Natural Science Foundation of China (No.: 21173226, 21376247), and State Key Laboratory of Multiphase Complex Systems, Institute of Process Engineering, Chinese Academy of Sciences (MPCS-2012-A-11, MPCS-2011-D-08, MPCS-2010-C-02) is gratefully acknowledged.

## Notes and references

<sup>a</sup> State Key Laboratory of Multiphase Complex Systems, Institute of Process Engineering, Chinese Academy of Sciences, Beijing, China 100190. Fax: 86-10-8254 4814; Tel: 86-10-8254 4915; E-mail: [jiang@mail.ipe.ac.cn](mailto:jiang@mail.ipe.ac.cn)

<sup>b</sup> University of Chinese Academy of Sciences, No. 19A Yuquan Road, Beijing, China 100049

<sup>c</sup> School of Engineering and Technology, China University of Geosciences, Beijing, China 100083

† Electronic Supplementary Information (ESI) available: XRD patterns, additional TEM, HRTEM, STEM images, element profiles, and EDX analyses for the characterization of the nanostructures in this study. See DOI:10.1039/b000000x/

- M. A. Mahmoud, C. E. Tabor, M. A. El-Sayed, Y. Ding and Z. L. Wang, *J. Am. Chem. Soc.*, 2008, **130**, 4590.
- Q. Shen, L. Jiang, H. Zhang, Q. Min, W. Hou and J.-J. Zhu, *J. Phys. Chem. C*, 2008, **112**, 16385.
- Z.-H. Lin, M.-H. Lin and H.-T. Chang, *Chem. Eur. J.*, 2009, **15**, 4656.
- M. Sanles-Sobrido, M. A. Correa-Duarte, S. Carregal-Romero, B. Rodríguez-González, R. A. Álvarez-Puebla, P. Hervés and L. M. Liz-Marzán, *Chem. Mater.*, 2009, **21**, 1531.
- A. Mohanty, N. Garg and R. A. Jin, *Angew. Chem., Int. Ed.*, 2010, **49**, 4962.
- Y. Fang, S. Guo, G. Zhu, S. Dong and E. Wang, *Langmuir*, 2010, **26**, 17816.
- L. Kuai, B. Geng, S. Wang and Y. Sang, *Chem. Eur. J.*, 2012, **18**, 9423.

- 8 F. Wang, C. Li, L.-D. Sun, C.-H. Xu, J. Wang, J. C. Yu and C.-H. Yan, *Angew. Chem., Int. Ed.*, 2012, **51**, 4872.
- 9 B. Lim, M. Jiang, P. H. C. Camargo, E. C. Cho, J. Tao, X. Lu, Y. Zhu and Y. Xia, *Science*, 2009, **324**, 1302.
- 10 Z. Peng and H. Yang, *J. Am. Chem. Soc.*, 2009, **131**, 7542.
- 11 S. Guo, S. Dong and E. Wang, *ACS Nano*, 2010, **4**, 547.
- 12 L. Wang, Y. Nemoto and Y. Yamauchi, *J. Am. Chem. Soc.*, 2011, **133**, 9674.
- 13 S. Mourdikoudis, M. Chirea, T. Altantzis, I. Pastoriza-Santos, J. Pérez-Juste, F. Silva, S. Bals, and L. M. Liz-Marzán, *Nanoscale*, 2013, **5**, 4776.
- 14 X. Zhong, Y. Feng, I. Lieberwirth and W. Knoll, *Chem. Mater.*, 2006, **18**, 2468.
- 15 X. Teng, X. Liang, S. Maksimuk and H. Yang, *Small*, 2006, **2**, 249.
- 16 L. Wang, C. Hu, Y. Nemoto, Y. Tateyama and Y. Yamauchi, *Cryst. Growth Des.*, 2010, **10**, 3454.
- 17 Y. Yamauchi, A. Tonegawa, M. Komatsu, H. Wang, L. Wang, Y. Nemoto, N. Suzuki and K. Kuroda, *J. Am. Chem. Soc.*, 2012, **134**, 5100.
- 18 S. Zhou, K. McIlwrath, G. Jackson and B. Eichhorn, *J. Am. Chem. Soc.*, 2006, **128**, 1780.
- 19 Z. Peng and H. Yang, *Nano Res.*, 2009, **2**, 406.
- 20 L. Wang and Y. Yamauchi, *J. Am. Chem. Soc.*, 2010, **132**, 13636.
- 21 Y. Feng, H. Liu and J. Yang, *J. Mater. Chem. A*, 2014, DOI: 10.1039/c3ta1421g.
- 22 W. F. McClune, *Powder Diffraction File Alphabetical Index Inorganic Phase*, JCPDS, Swarthmore, PA, 1980.
- 23 H. Hiramatsu and F. E. Osterloh, *Chem. Mater.*, 2004, **16**, 2509.
- 24 H. Yu, M. Chen, P. M. Rice, S. X. Wang, R. L. White and S. Sun, *Nano Lett.*, 2005, **5**, 379.
- 25 Z. Li, J. Tao, X. Lu, Y. Zhu and Y. Xia, *Nano Lett.*, 2008, **8**, 3052.
- 26 Z. Xu, C. Shen, Y. Hou, H. Cao and S. Sun, *Chem. Mater.*, 2009, **21**, 1778.
- 27 S. Mourdikoudis and L. M. Liz-Marzán, *Chem. Mater.*, 2013, **25**, 1465.
- 28 X. Liu, M. Atwater, J. Wang, Q. Dai, J. Zou, J. P. Brennan and Q. Huo, *J. Nanosci. Nanotechnol.*, 2007, **7**, 3126.
- 29 W. F. Ostwald, *Z. Phys. Chem.*, 1897, **22**, 289.
- 30 Z. Peng, J. Wu and H. Yang, *Chem. Mater.*, 2010, **22**, 1098.
- 31 R. Liu, H. Iddir, Q. Fan, G. Hou, A. Bo, K. L. Ley and E. S. Smotkin, *J. Phys. Chem. B*, 2000, **104**, 3518.
- 32 J. H. Jiang and A. Kucernak, *Electrochem. Commun.*, 2009, **11**, 1005.
- 33 K. L. Ley, R. Liu, C. Pu, Q. Fan, N. Leyarovska, C. Segre and E. S. Smotkin, *J. Electrochem. Soc.*, 1997, **144**, 1543.
- 34 M. Watanabe and S. Motoo, *J. Electroanal. Chem.*, 1975, **60**, 267.
- 35 M. Watanabe and S. Motoo, *J. Electroanal. Chem.*, 1975, **60**, 275.

Graphical abstract

## A universal approach to the synthesis of nanodendrites of noble metals

Yan Feng,<sup>ab</sup> Xiaohong Ma,<sup>a</sup> Lin Han,<sup>c</sup> Zhijian Peng<sup>c</sup> and Jun Yang<sup>a\*</sup>

A universal approach was demonstrated for the synthesis of noble metal nanoparticles with dendritic structures.

